The star formation history of the Magellanic Clouds derived from long-period variable star counts

Sara Rezaei kh.,[1][*] Atefeh Javadi,[1][*] Habib Khosroshahi[1] and Jacco Th. van Loon[2]

[1]*School of Astronomy, Institute for Research in Fundamental Sciences (IPM), PO Box 19395-5531 Tehran, Iran*
[2]*Lennard-Jones Laboratories, Keele University, Keele, Staffordshire ST5 5BG, UK*

ABSTRACT

We present the first reconstruction of the star formation history (SFH) of the Large and Small Magellanic Clouds (LMC and SMC) using Long Period Variable stars. These cool evolved stars reach their peak luminosity in the near-infrared; thus, their K-band magnitudes can be used to derive their birth mass and age, and hence the SFH can be obtained. In the LMC, we found a 10-Gyr old single star formation epoch at a rate of ~ 1.5 $M_\odot$ yr^{-1}, followed by a relatively continuous SFR of ~ 0.2 $M_\odot$ yr^{-1}, globally. In the core of the LMC (LMC bar), a secondary, distinct episode is seen, starting 3 Gyr ago and lasting until ~ 0.5 Gyr ago. In the SMC, two formation epochs are seen, one ~ 6 Gyr ago at a rate of ~ 0.28 $M_\odot$ yr^{-1} and another only ~ 0.7 Gyr ago at a rate of ~ 0.3 $M_\odot$ yr^{-1}. The latter is also discernible in the LMC and may thus be linked to the interaction between the Magellanic Clouds and/or Milky Way, while the formation of the LMC bar may have been an unrelated event. Star formation activity is concentrated in the central parts of the Magellanic Clouds now, and possibly has always been if stellar migration due to dynamical relaxation has been effective. The different initial formation epochs suggest that the LMC and SMC did not form as a pair, but at least the SMC formed in isolation.

Key words: stars: evolution – stars: luminosity function, mass function – Magellanic Clouds – galaxies: star formation – galaxies: stellar content – galaxies: structure.

1 INTRODUCTION

The Magellanic Clouds (Large, LMC, and Small, SMC) are irregular, gas-rich dwarf galaxies in our Local Group. The presence of a bar-like structure – especially prominent in the LMC – suggests that they could have originally been barred spiral galaxies transformed into present-day irregular galaxies due to their tidal interactions with one another and with the Milky Way. At a distance of 48.5 kpc (Macri et al. 2006; Freedman, Kennicutt & Mould 2010), the LMC is the third closest galaxy to the Milky Way. With an inclination of 32° (Haschke, Grebel & Duffau 2011), it offers us an excellent view of its structure and content. The SMC is located at a distance of ~ 61 kpc (Hilditch, Howarth & Harries 2005) with an inclination of only 2°.6 (Subramanian & Subramanian 2011).

Probing the star formation history (SFH) in galaxies informs us about galaxy formation and evolution. Star clusters revealed differences in the SFH between the LMC and the Milky Way (Hodge 1960; Sagar & Pandey 1989): the LMC contains a larger fraction of young clusters relative to the Milky Way. Other methods of determining the SFH include a comparison of the observed colour–magnitude diagrams (CMDs) with the model-built CMDs (e.g. Bertelli et al. 1992). Harris & Zaritsky (2009) used multicolour photometry of millions of stars over ≈ 65 deg^2 of the LMC to derive the SFH; they found multiple episodes of star formation between 5 and 0.1 Gyr ago in addition to an initial burst of star formation ~ 12 Gyr ago. In a recent study, Cignoni et al. (2013) studied various fields within the bar and wing of the SMC and confirmed a dominant intermediate-age star formation epoch. Their derived metallicity for the fields support a well-mixed metal content of the SMC. The CMD approach has also revealed that the most recent star formation, as young as ≈ 100 Myr, is confined to the central regions in both the LMC and SMC (Indu & Subramanian 2011).

Our approach to investigate the SFH is based on employing long-period variable stars (LPVs). These are mostly asymptotic giant branch (AGB) stars at their very late stage of evolution, as well as more massive red supergiants (RSGs). The AGB stars alone have low- to intermediate-mass ranges which relate to diverse ages and hence time epochs in the past, and they can thus be used to derive star formation rates (SFRs) over much of a galaxy's cosmological evolution. The AGB stars develop unstable mantles which cause radial pulsation at periods of one or a few years (e.g. Wood et al. 1992; Whitelock et al. 2003); they are luminous ($\sim 10^4$ L$_\odot$) and cool (< 4000 K) and hence stand out at near-infrared wavelengths.

[*] E-mail: s.rezaei.kh@gmail.com (SR); atefeh@ipm.ir (AJ)

Their colours can be further reddened by enhanced atmospheric opacity due to carbon-dominated chemistry (in carbon stars) or due to attenuation by circumstellar dust produced in their winds (e.g. van Loon et al. 1997, 2008). Thanks to recent large-scale, extended monitoring projects such as OGLE-I, II, III, MACHO, and others, we are now in a position to use LPVs to study these nearby galaxies.

The data and the methodology are described in Section 2. In Section 3, we present our analysis and the results. In Section 4, we present the SFH derived from our analysis. Section 5 presents a discussion of the findings and a comparison with other studies. Section 6 contains a summary and conclusions.

2 DATA AND METHODOLOGY

In this paper, we use the catalogue of LPVs in the LMC from Spano et al. (2011) and in the SMC from Soszyński et al. (2011). In the case of the LMC, they used the EROS-2 survey which started functioning efficiently from 1996; it employed two cameras enabling observations at two wavelengths, blue (BE) and red (RE), simultaneously. After seven years of monitoring, it provided a data base of 856 864 variables in the LMC of which 43 551 are considered LPVs (Spano et al. 2011). The EROS-2 survey covered an area of 88 deg^2 on the LMC, which is a superior coverage in comparison with other projects such as MACHO and OGLE-III which covered areas on the LMC of 13.5 and 40 deg^2, respectively.

Spano et al. cross-identified the EROS-2 LPV candidates with variable stars from the OGLE-III and MACHO surveys. They found nearly 60 per cent of LPVs in common between EROS-2 and MACHO; the difference is attributed to differences in sky coverage between the surveys (Spano et al. 2011). For the SMC, Soszyński et al. used the OGLE-III project which has monitored an area of 14 deg^2 on the SMC. After 13 yr of monitoring in the optical *V*- and near-infrared *I*-band, the OGLE survey has provided a data base of about 6 million stars in the SMC of which 19 384 identified as LPVs are detected (Soszyński et al. 2011).

As mentioned, AGB stars become surrounded by dust, which causes reddening and makes them particularly faint in optical bands. Therefore, infrared (IR) studies are preferred. For a comparison and more detailed study of the core region, we also utilize the Ita et al. (2004a) data of variable stars in the Magellanic Clouds. This catalogue had been obtained by cross-identifying the OGLE-II and SIRIUS data (simultaneously observed in *J*, *H*, and *K* band). The total area covered by the SIRIUS survey is 3 and 1 deg^2 in the LMC and SMC, respectively, covering the core region of these galaxies – in particular, the bar of the LMC (see Fig. 1). Spano et al. (2011) cross-matched the EROS-2 survey with 2MASS near-IR (and *Spitzer* mid-IR) data, within a search radius of 1 arcsec. For the SMC, we cross-matched the original catalogue of Soszyński et al. (2011) with 2MASS, also within a search radius of 1 arcsec.

Ita et al. classified the variable stars into nine groups for the LMC and eight groups for the SMC, based on their location in the period – *K*-band magnitude plane. The categories include Cepheids, Miras, semi regulars, irregular variables and eclipsing binaries (Ita et al. 2004a). In total, the number of variable stars in Ita's catalogues of the LMC and SMC are 8852 and 2927, respectively. For the purpose of this study, we select LPVs pulsating in the fundamental mode, equal to sequences C and D in Ita et al. (2004a) above the (first ascent) red giant branch (RGB) tip ($K \sim 12$ and ~ 12.7 mag for the LMC and SMC, respectively). Spano et al. (2011) classified their variable stars using period–luminosity relations ($\log P - K$ diagram), into six groups (figs 22 and 23 in their paper), from which sequence C is considered as Miras pulsating in the fundamental mode. Sequence D comprises mostly of stars with secondary long periods that are probably not due to the same radial pulsation we are after, but it does contain some dusty LPVs that have lengthened pulsation periods as a result of diminished mass (Ita et al. 2004b; Spano et al. 2011). For the purpose of this study, we select variables belonging to sequence C, and variables with 'only' one period in sequence D.

An appropriate stellar evolution model is provided by the Padova group (Marigo et al. 2008). LPVs are expected to be at the
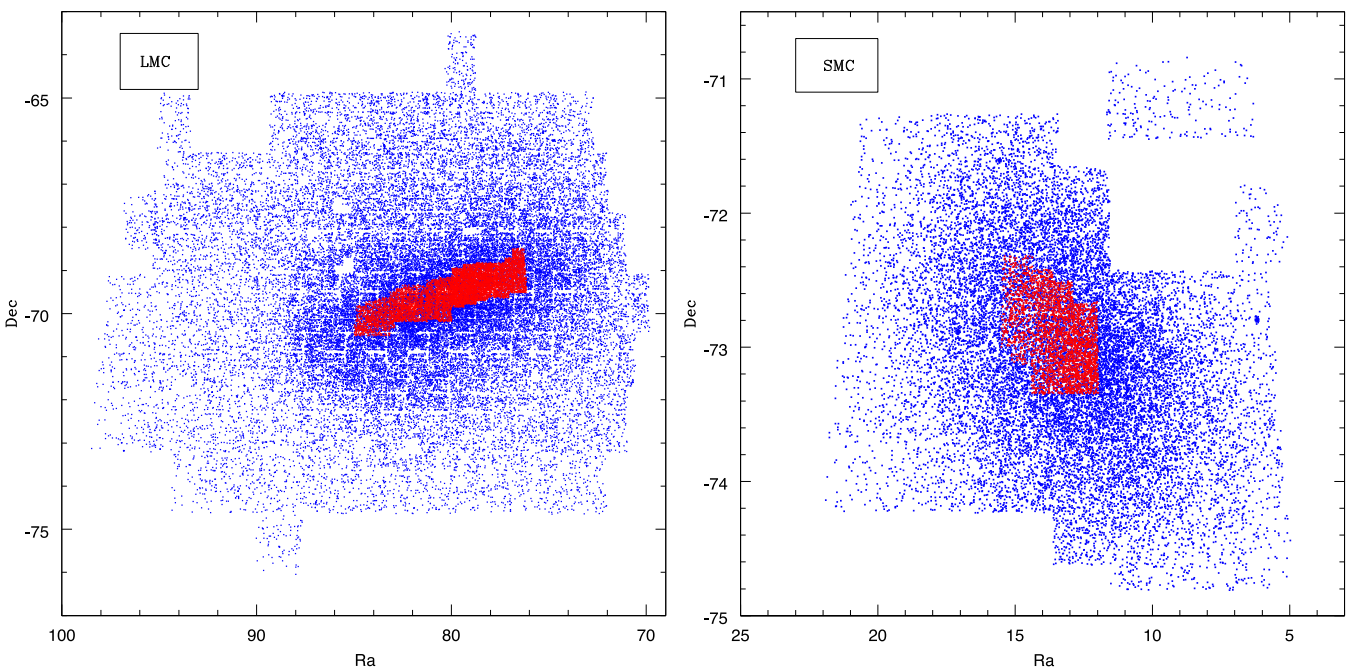

Figure 1. Left: spatial coverage of the Spano et al. (2011) survey (blue) and Ita et al. (2004a) survey (red) in the LMC. Right: spatial coverage of the Soszyński et al. (2011) survey (blue) and Ita et al. (2004a) survey (red) in the SMC.
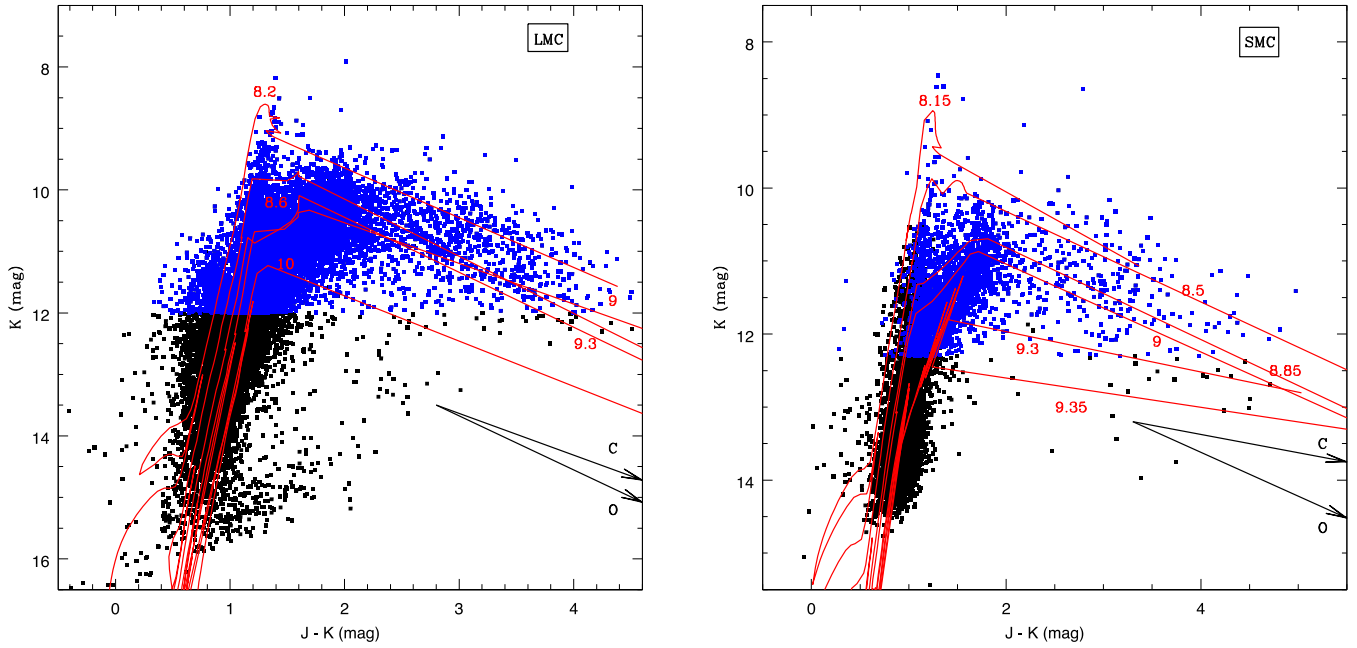
Figure 2. CMD of the LMC (left) and SMC (right), overlain with Marigo et al. (2008) isochrones (labelled by logarithmic age in yr); among with circumstellar reddening vectors for oxygenous and carbonaceous dust (O and C, respectively), explained in Section 3.1.1. Blue points represent stars above the RGB-tip.

end-points of the AGB (or RSG) part of the isochrones in CMDs. Thus, the Padova isochrones were fitted to the CMDs of the Magellanic Clouds in order to correct the reddened LPVs (see Fig. 2). Two different groups of reddening slopes are seen, those with steeper slopes are associated with those stars surrounded by oxygenous dust whilst some with shallower slopes are associated with carbonaceous dust. Not all stars are reddened; the correction is applied only to those stars which have $J - K > 1.5$ mag.

3 FROM K-BAND MAGNITUDE TO THE STAR FORMATION HISTORY

The total mass of stars formed between t and $t + \mathrm{d}t$ depends on star formation rate (SFR), $\xi(t)$, as

$$\mathrm{d}M(t) = \xi(t)\,\mathrm{d}t. \qquad (1)$$

Thus, N, the number of stars formed, is defined by the following equation

$$\mathrm{d}N(t) = \left[\frac{\int_{\min}^{\max} f_{\mathrm{IMF}}(m)\,\mathrm{d}m}{\int_{\min}^{\max} f_{\mathrm{IMF}}(m)m\,\mathrm{d}m} \right] \mathrm{d}M(t), \qquad (2)$$

in which f_{IMF} is the initial mass function. The nominator represents the total number of stars within the mass range of $M_{\min}$–$M_{\max}$, whilst the denominator gives their total mass. Therefore, the fraction refers to the number of stars per mass unit. For the initial mass function, the Kroupa (2001) model was used, where we assumed $M_{\min} = 0.02\,\mathrm{M_\odot}$ and $M_{\max} = 200\,\mathrm{M_\odot}$. The number of stars formed between t and $t + \mathrm{d}t$ is then obtained as follows:

$$\mathrm{d}n(t) = \left[\frac{\int_{m(t)}^{m(t+\mathrm{d}t)} f_{\mathrm{IMF}}(m)\,\mathrm{d}m}{\int_{\min}^{\max} f_{\mathrm{IMF}}(m)\,\mathrm{d}m} \right] \mathrm{d}N(t). \qquad (3)$$

Because the large-amplitude, long-period variability only comprises a short phase in the evolution of a star lasting δt, the number of such variable stars that were formed is reduced to

$$\mathrm{d}n'(t) = \left[\frac{\delta t}{\mathrm{d}t} \right] \mathrm{d}n(t). \qquad (4)$$

Thus, the final equation for the SFR derived from the variable star counts is

$$\xi(t) = \left[\frac{\int_{\min}^{\max} f_{\mathrm{IMF}}(m)m\,\mathrm{d}m}{\int_{m(t)}^{m(t+\mathrm{d}t)} f_{\mathrm{IMF}}(m)\,\mathrm{d}m} \right] \frac{\mathrm{d}n'(t)}{\delta t}. \qquad (5)$$

3.1 From K-band magnitude to age

For reasons that will become clear below, we convert K-band magnitudes into stellar birth mass, first, before converting that into the age of the star. For the latter, we use the following mass–age relation

$$\log t\,[\mathrm{yr}] = a \log M\,[\mathrm{M_\odot}] + b, \qquad (6)$$

where a and b are given in Javadi, van Loon & Mirtorabi (2011), based on the models from Marigo et al. (2008).

Javadi et al. (2011) give the mass–luminosity (K-band magnitude) relation as

$$\log M\,[\mathrm{M_\odot}] = aK + b, \qquad (7)$$

where K is the (extinction-corrected) K-band magnitude and a and b are defined in Table 1 for various ranges of K. We use a distance modulus of $\mu = 18.5$ (Luri et al. 1998; Gieren et al. 2005) and $\mu = 18.9$ mag for the LMC and SMC, respectively.

3.1.1 Dust correction

The light from the variable stars can be attenuated by interstellar and/or circumstellar dust; this is wavelength dependent resulting also in reddening of the near-IR colours. To determine the intrinsic

Table 1. Mass–luminosity relation, $\log M\,[\mathrm{M}_\odot] = aK + b$, valid for the Large ($Z = 0.008$) and Small ($Z = 0.004$) Magellanic Clouds (Javadi et al. 2011).

a	b	Validity range
	$Z = 0.008$	
-0.840	12.840	$K \leq 7.332$
-0.589	9.391	$7.332 < K \leq 8.387$
-0.188 ± 0.028	3.465 ± 0.043	$8.387 < K \leq 8.900$
-0.142 ± 0.027	2.758 ± 0.041	$8.900 < K \leq 9.413$
-0.188 ± 0.022	3.487 ± 0.036	$9.413 < K \leq 9.927$
-0.501 ± 0.016	8.183 ± 0.024	$9.927 < K \leq 10.440$
-0.248 ± 0.018	4.335 ± 0.026	$10.440 < K \leq 10.953$
-0.128 ± 0.025	2.257 ± 0.035	$K > 10.953$
	$Z = 0.004$	
-0.708	11.1268	$K \leq 8.734$
-0.209 ± 0.051	3.783 ± 0.077	$8.734 < K \leq 9.140$
-0.240 ± 0.054	4.244 ± 0.078	$9.140 < K \leq 9.545$
-0.050 ± 0.060	1.291 ± 0.091	$9.545 < K \leq 9.951$
-0.131 ± 0.054	2.583 ± 0.083	$9.951 < K \leq 10.356$
-0.243 ± 0.041	4.409 ± 0.057	$10.356 < K \leq 10.762$
-0.714 ± 0.039	12.310 ± 0.055	$10.762 < K \leq 11.167$
-0.109 ± 0.043	1.932 ± 0.070	$11.167 < K \leq 11.573$
-0.153 ± 0.046	2.690 ± 0.067	$K > 11.573$

K-band magnitude, the photometry needs to be de-reddened. The (de-)reddening slope in the CMD depends on whether the dust is oxygenous or carbonaceous in composition. Stars with a birth mass in the range of 1.5–4 $\mathrm{M}_\odot$ are expected to have become carbon stars due to the third dredge-up of nuclear-processed material with a carbon:oxygen ratio in excess of unity. In stars with a birth mass <1.5 $\mathrm{M}_\odot$, third dredge-up is not sufficiently efficient, whilst, for stars with a birth mass >4 $\mathrm{M}_\odot$ nuclear burning of the carbon at the

bottom of the convection zone prevents the surface to be enriched in carbon. The reddening correction equation is

$$K = K + a(1.25 - (J - K)), \tag{8}$$

where a is the average slope for each dust type.

The procedure followed was to first apply a correction assuming carbonaceous dust. If the mass resulting from this corrected K-band magnitude ended up in the range 1.5–4 $\mathrm{M}_\odot$, then the star was treated as a carbon star. Otherwise, the correction was replaced by one assuming oxygenous dust, and a mass was derived accordingly.

Fig. 3 shows the mass histogram for different choices of reddening correction. To appreciate the impact of these choices on the derived SFH, we also applied the reverse approach; assuming that stars are oxygen-rich unless their masses would fall within 1.5–4 $\mathrm{M}_\odot$.

3.2 The fraction of the time spent pulsating

Equation (5) depends on a correction factor (δt) for the duration of the evolutionary phase in which the star exhibits large-amplitude, long-period pulsations. Generally, since a massive star evolves faster, its pulsation duration is shorter. Thus, low-mass stars are more likely to be identified as variables, in comparison to more massive stars. However, the pulsation phase depends sensitively on the star's effective temperature which, in turn, depends on metallicity, mass-loss, et cetera.

The mass–pulsation relation from Javadi et al. (2011) is used to connect the birth mass of stars to their pulsation duration. Relative to its age, it is parametrized as

$$\log\left(\frac{\delta t}{t}\right) = D + \sum_{i=1}^{3} a_i \exp\left[\frac{\left(\log M\,[\mathrm{M}_\odot] - b_i\right)^2}{2c_i^2}\right], \tag{9}$$

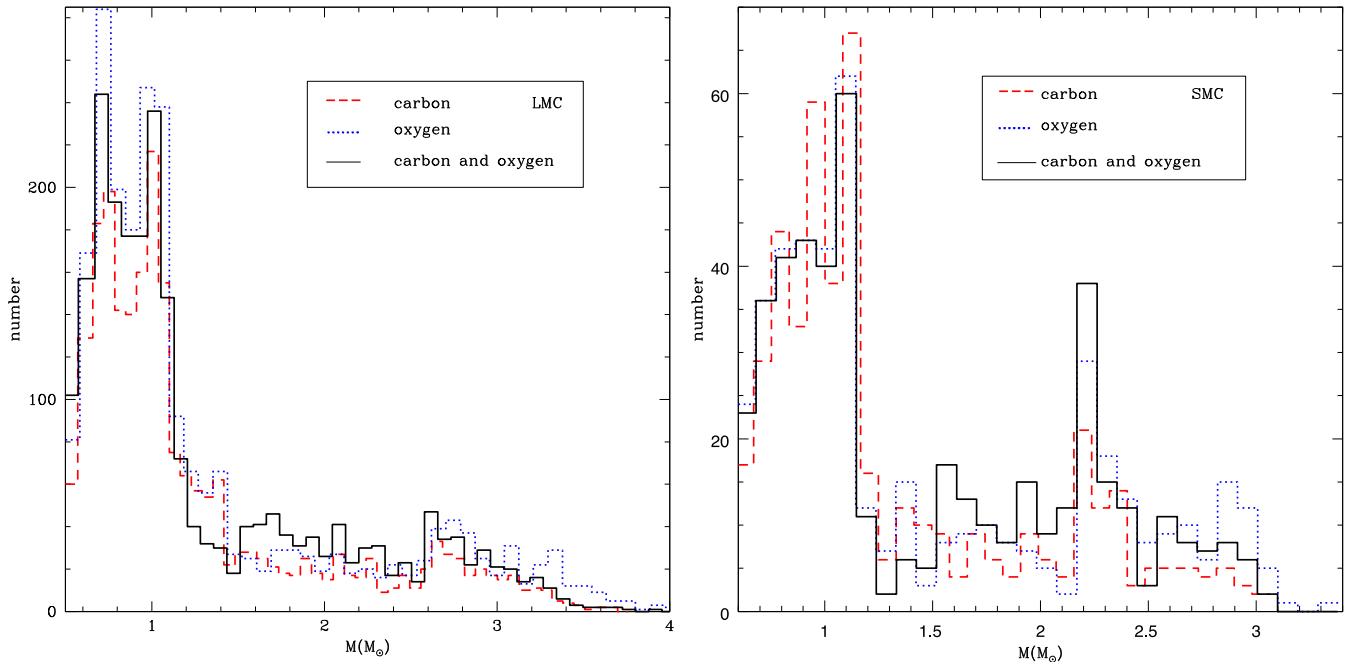where a, b, c, and D are defined in Table 2.

Figure 3. Present-day mass function of the LMC (left) and SMC (right). The red dashes represent related to carbonaceous correction only, the blue dots represent oxygenous correction only, and the black lines refer to the approach described in the text applying carbonaceous and oxygenous corrections depending on the resulting mass.

Table 2. Parameters adopted for the mass–pulsation relation, $\log(\delta t/t) = D + \sum_{i=1}^{3} a_i \exp\left((\log M\,[\mathrm{M}_\odot] - b_i)^2/(2c_i^2)\right)$, where δt is the pulsation duration and t is the age of the star, for the Large ($Z = 0.008$) and Small ($Z = 0.004$) Magellanic Clouds (Javadi et al. 2011).

D	i	a	b	c
		$Z = 0.008$		
-3.96	1	2.34	1.281	0.378
	2	1.32	0.460	0.165
	3	0.38	0.145	0.067
		$Z = 0.004$		
-4.00	1	2.29	1.217	0.408
	2	0.84	0.524	0.093
	3	0.87	0.206	0.088

Given the above argument, the SFR estimated using LPVs is shown to be underestimated by a factor of 10 (Javadi et al. 2013) in comparison to the SFR obtained using Hα emission, for instance. This inaccuracy was exposed by a mismatch between the integrated mass-loss and birth mass. To reconcile both the mass-loss budget and SFR with independent evidence, the pulsation duration adopted from the Marigo et al. (2008) models needs to be decreased by a factor 10. This is a fairly robust result and we thus apply the correction in our work. Given the uncertainties in the models, in particular with regard to the duration of the LPV phase, the SFRs and stellar masses formed are possibly uncertain by up to a factor of a few.
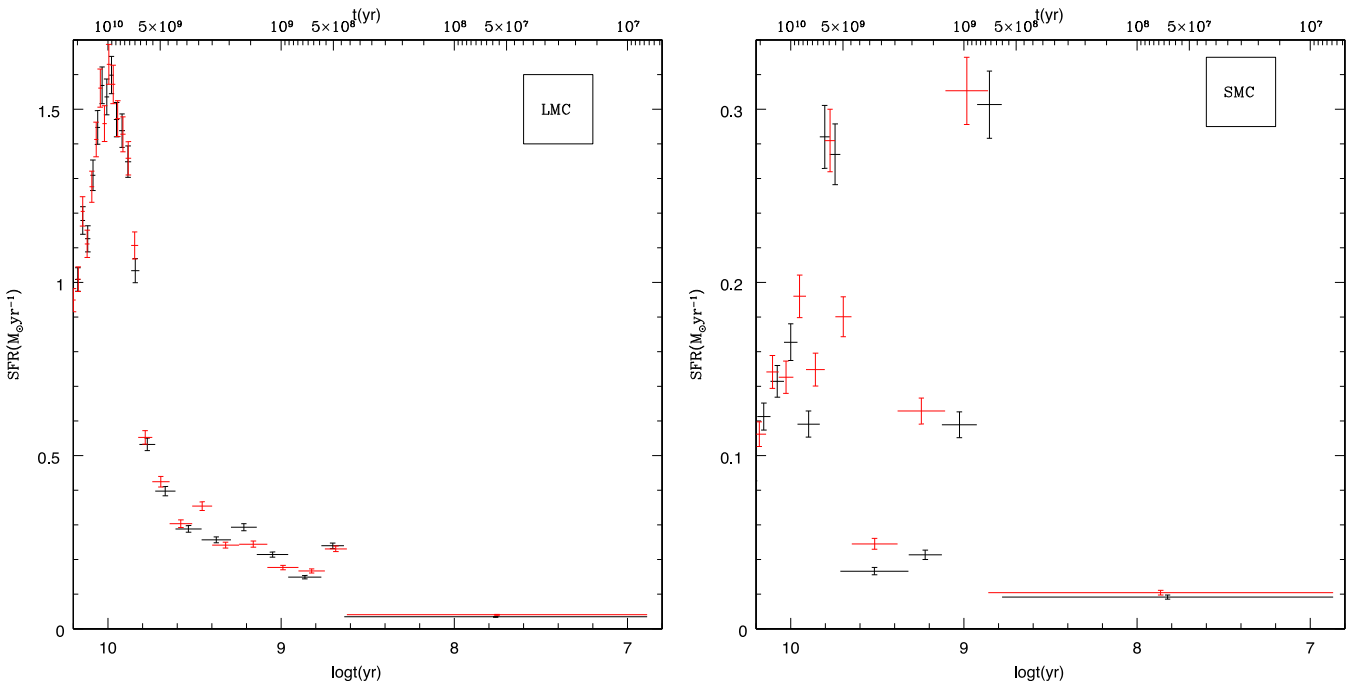
4 RESULTS AND DISCUSSION

4.1 The global SFH of the Magellanic Clouds

We thus derive the SFRs as a function of time, where we group the stars into bins of equal numbers – i.e. equal Poissonian significance. Fig. 4 represents the SFHs for both reddening correction approaches (see Section 3.1.1); black lines indicate the case in which a carbonaceous-dust correction is first applied, and red lines demonstrate the reverse – however, there is no noticeable difference in the SFRs between these two correction approaches. Horizontal lines show time bins while vertical lines demonstrate statistical error bars derived as following;

$$\sigma_\xi = \frac{\sqrt{N}}{N}\,\xi,\tag{10}$$

where 'N' is the number of stars in each age bin. For the LMC (Fig. 4, left-hand panel), we find an ancient star formation episode with rate of $1.598 \pm 0.054\ \mathrm{M}_\odot\ \mathrm{yr}^{-1}$ ∼10 Gyr ago ($\log t = 10$), corresponding to the formation of the LMC: the total stellar mass produced in the LMC is ∼$2.2 \times 10^{10}\ \mathrm{M}_\odot$, of which ≈89 per cent was formed during the first epoch. For the SMC (Fig. 4, right-hand panel), two formation epochs are observed; one with an SFR of $0.282 \pm 0.017\ \mathrm{M}_\odot\ \mathrm{yr}^{-1}$ rate ∼6 Gyr ago ($\log t = 9.8$) and a secondary star formation episode ∼0.7 Gyr ago ($\log t = 8.8$) with a similar SFR of $0.310 \pm 0.019\ \mathrm{M}_\odot\ \mathrm{yr}^{-1}$. These findings are in good agreement with recent studies, e.g. Weisz et al. (2013). Of a total stellar mass in the SMC of ∼$4.0 \times 10^8\ \mathrm{M}_\odot$, ≈82 per cent was produced during the first peak in SFR, and ≈11 per cent during the second peak.

Figure 4. Global SFH of the LMC (left) and SMC (right) using both reddening correction approaches; black lines represent applying a carbonaceous-dust correction first, whilst red lines demonstrate the reverse (see Section 3.1.1). Vertical lines show statistical error bars described in equation (10). For the LMC, an initial burst of star formation as old as 10 Gyr is observed ($\log t = 10$), with an SFR of ∼1.5 M$_\odot$ yr^{-1}, followed by more quiescent star formation. In the case of the SMC, an initial burst of star formation as old as 6 Gyr is observed ($\log t = 9.8$), with an SFR of ∼0.28 M$_\odot$ yr^{-1}, followed by a secondary star formation epoch ∼0.7 Gyr ago ($\log t = 8.8$) with an SFR of ∼0.3 M$_\odot$ yr^{-1}.
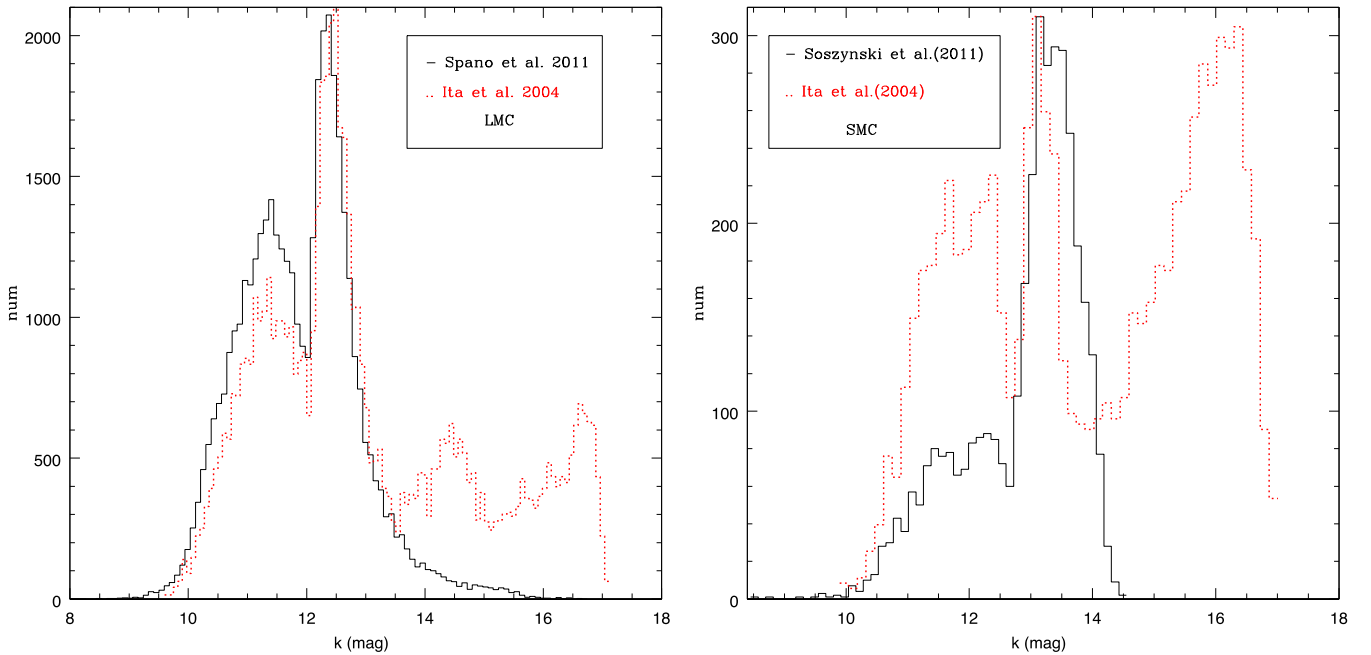
Figure 5. *K*-band histograms for variable stars in the overlapping regions (see Fig. 1) in the central parts of the LMC (left) and SMC (right), from Ita et al. (2004a; red dotted lines), and from Spano et al. (2011) and Soszyński et al. (2011; solid black lines) in the LMC and SMC, respectively. Each peak shows a type of variables, from left to right: AGB stars, RGB stars, and Cepheids.

4.2 SFH of the central regions

Before investigating the SFH in the central regions of the LMC and SMC, and comparing it to the SFH in their peripheries, we consider the use of the Ita et al. (2004a) catalogue for the central regions. Fig. 5 shows the normalized *K*-band luminosity distributions. The peak at the brightest *K*-band magnitudes corresponds to the AGB; the second peak starts at $K \sim 12$ mag for the LMC and $K \sim 12.7$ mag for the SMC, which corresponds to the RGB tip. The deeper Ita et al. catalogue also contains fainter stars including Cepheids. For the purpose of our study, based mainly on AGB stars (and small numbers of RSGs) there is no indication that the IR catalogue of Ita et al. of the LMC variables offers any major advantage over the Spano et al. (2011) catalogue (we remind the reader that the latter is originally an optical catalogue cross matched with 2MASS). On the other hand, in the central part of the SMC, the Ita et al. catalogue is preferred over that of Soszyński et al. (2011) as the former is much more complete for the AGB stars.

The SFH of the LMC was derived from the Ita et al. (2004a) catalogue, and for the overlapping region with the Spano catalogue (left-hand panel in Fig. 6). This area corresponds to the bar structure of the LMC (see Fig. 1). For a meaningful comparison with the literature, we report the SFR per physical area. The SFR in the LMC bar varies from ~ 0.01 to 0.1 M$_\odot$ yr^{-1} kpc^{-2}. Two formation epochs are seen; one epoch ~ 10 Gyr ago ($\log t = 10$) when almost 48 per cent of the total stellar mass within the bar was formed, and a more recent epoch starting ~ 3 Gyr ago ($\log t = 9.4$) which lasted until as recent as 500 Myr ago ($\log t = 8.7$), within which almost 30 per cent of the total stellar mass was formed (the total stellar mass in the covered area is $\sim 1.4 \times 10^8$ M$_\odot$). These two estimates are consistent between the use of both catalogues, except for the ancient epoch in which a higher SFR is found for the Spano data. However, it appears as though the SFR based on Spano et al. (2011) is more successful in recovering the ancient star formation. Cioni et al. (2014) also found the SFH of the LMC using

Vista survey of the Magellanic Clouds which reported an old star formation at around $\log t = 9.9$ as well as a secondary peak of star formation at $\sim \log t = 8.5$–8.7 for stars closer to the LMC centre. These two peaks in SFR coincide with the peaks that we have determined, though we argue for a more sustained star formation over the most recent few Gyr.

The SFH of the SMC based on the Ita et al. (2004a) catalogue was also derived and compared with that derived for the overlapping region in the Soszyński et al. (2011) catalogue (right-hand panel in Fig. 6). This corresponds to the central, approximately square-degree region of the SMC (see Fig. 1). The SFR varies from ~ 0.006 to ~ 0.07 M$_\odot$ yr^{-1} kpc^{-2}. As in other studies (e.g. Cignoni et al. 2012), two formation episodes can be identified; one episode ~ 6 Gyr ago ($\log t = 9.8$) when almost 49 per cent of the total stellar mass was formed, and another one ~ 800 Myr ago ($\log t = 8.9$) within which around 12 per cent of the total stellar mass was formed. As for the LMC, the SFRs obtained for both catalogues agree rather well, however, the Ita et al. data indicate a relatively more pronounced secondary (recent) episode of star formation.

By excluding the stars in the bar/central regions of the galaxies (amounting to 3 and 1 deg^2 in the LMC and SMC, respectively), we also obtained the SFH for the outer regions. Conversely, we also isolated the SFH of the bar/central regions by subtracting that derived for the immediately surrounding regions (which could also be seen in projection against and/or mixed with any distinct SFHs belonging to the bar/central regions). Fig. 7 shows a comparison between the SFHs derived for the different regions. In case of the LMC, the second peak of star formation is not seen in the outer region whilst for the SMC, another remarkable peak of star formation is still observed in outer region. The latter is in good agreement with the work by Ripepi et al. (2014) who, using the optical STEP survey, found regions of high levels of star formation in the north and in the Wing of the SMC.
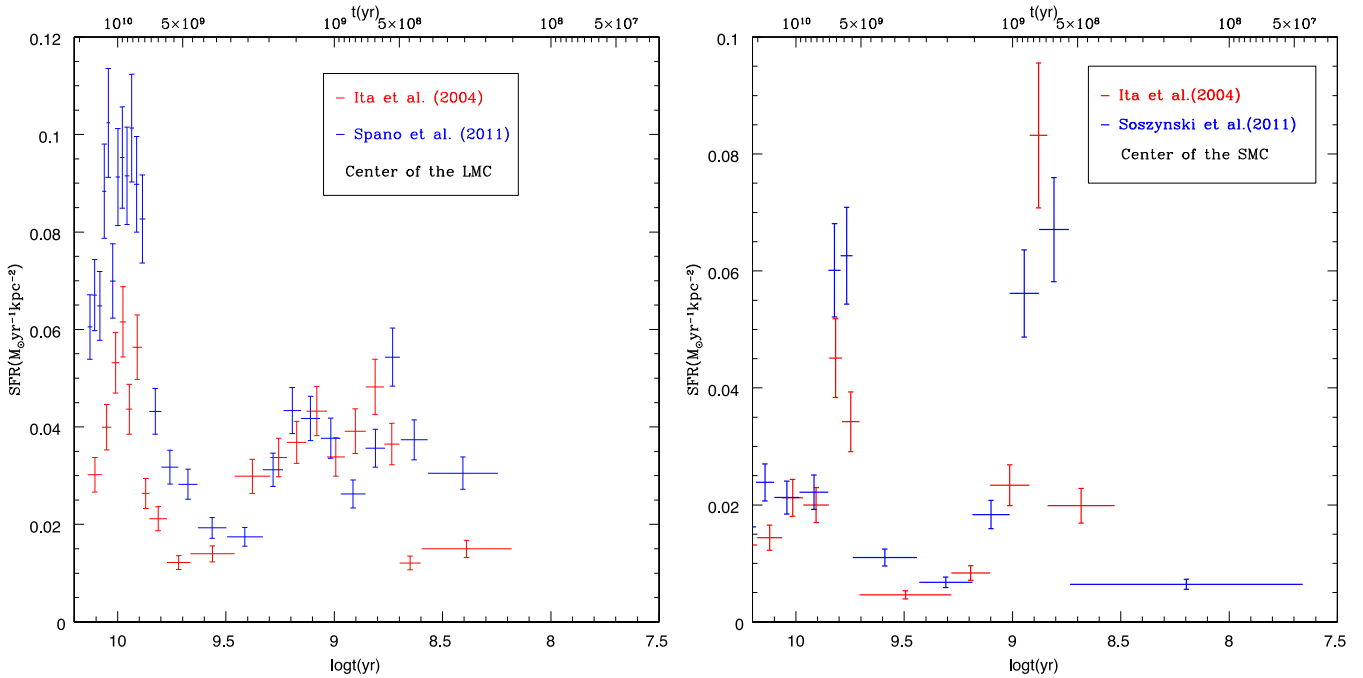
Figure 6. Left: SFH of the central bar structure in the LMC based on the catalogues of Ita et al. ([2004a](); red symbols) and Spano et al. ([2011](); blue symbols); along with statistical error bars discussed in Section 4.1. The Spano et al. data indicate a higher rate of initial star formation, by a factor of 2 compared to the Ita et al. data. However, the two data sets agree well on the more recent SFRs. Right: SFH of the overlapping region at the centre of the SMC based on the catalogues of Ita et al. ([2004a](); red symbols) and Soszyński et al. ([2011](); blue symbols). The Ita et al. data imply a higher rate of secondary star formation, whilst the Soszyński et al. data imply relatively higher rates during the initial star formation episode.
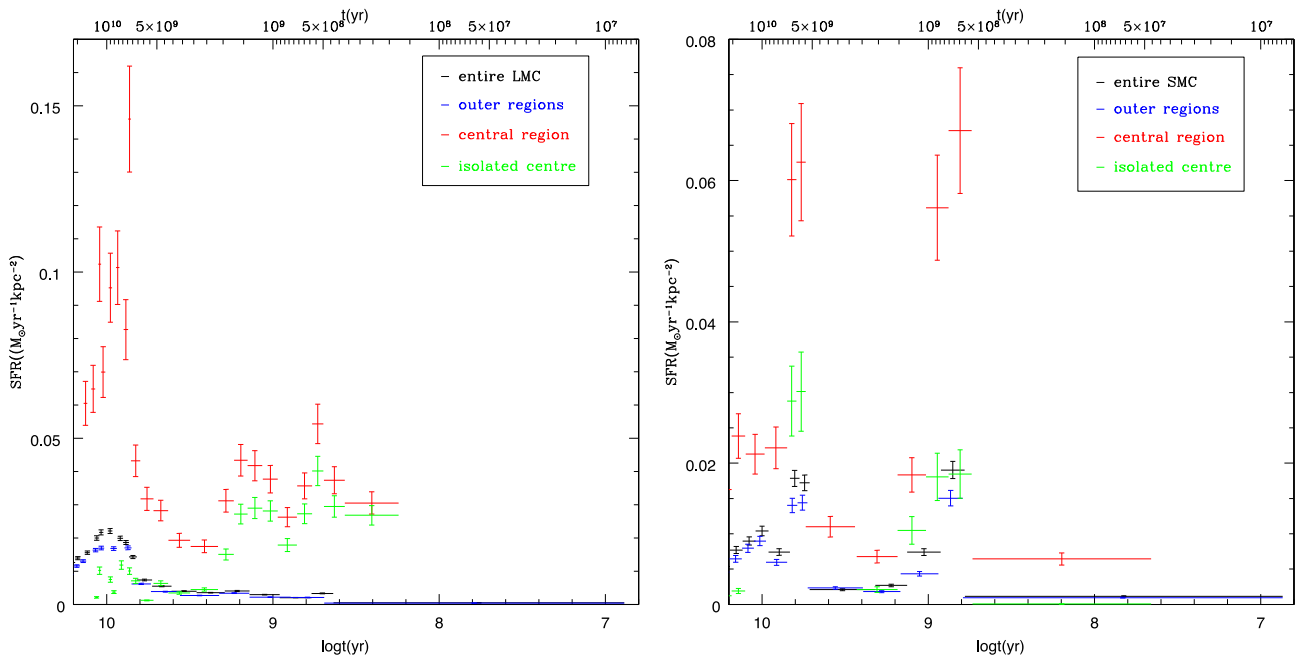

Figure 7. SFHs based on LPVs in the catalogues of Spano et al. ([2011]()) for the LMC (left) and Soszyński et al. ([2011]()) for the SMC (right). Black symbols: global star formation; blue symbols: star formation in the outskirts of the galaxies; red symbols: bar (for the LMC) and central (for the SMC) star formation; and green symbols: isolated star formation for the central regions derived by subtracting the SFH of the surrounding parts; along with statistical error bars explained in Section 4.1. For both galaxies, the bar/central star formation is remarkably dominant.

Fig. [8]() shows the ratio of the SFR in the central regions compared to that in the outer regions. Each bin in the histograms contains an equal number of stars. Note also the logarithmic scale. The LMC shows a steady concentration of younger stars in the central regions (Monelli et al. [2011]()). A similar result was reported by Meschin

et al. ([2014]()), who found an ancient star formation epoch dating back 10 Gyr, followed by more recent star formation activity 4–1 Gyr ago. They also found younger stellar populations to be more centrally concentrated; in other words, the stellar population ages as one moves away from the centre of the galaxy. Any such trend in
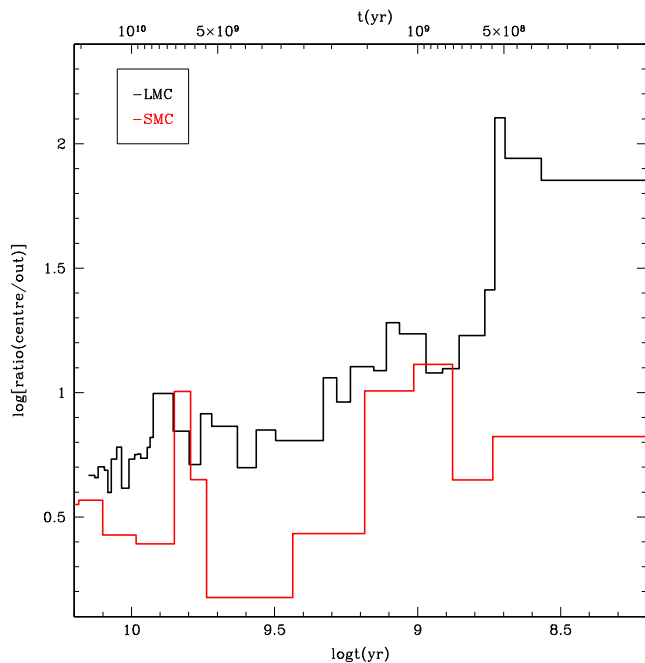
Figure 8. Ratio of the SFR in the centre compared to that in the outskirts, for the LMC (in black) and SMC (in red). Each bin in the histogram contains an equal number of stars. Clearly, star formation activity has been centrally concentrated in recent times, and possible always if old stars have migrated to the outskirts.

the SMC is less obvious, though might also be present. Dynamical effects will have resulted in the migration of old stars towards the outskirts, so it is impossible to tell on the basis of this work whether star formation activity has always been centrally concentrated, or whether it has progressed further inwards as the galaxies matured. As the dynamical time-scale is not much more than 100 Myr, stars that were formed more than a Gyr ago will have equilibrated their kinematics with the gravitational potential well – unless they have been exposed to recent tidal disturbances.

5 CONCLUDING REMARKS

We find a significant difference in the ancient SFH of the LMC and the SMC. For the LMC, the bulk of the stars formed ≈10 Gyr ago, while the strongest episode of star formation in the SMC occurred a few Gyr later. This is consistent with the findings of Weisz et al. (2013) obtained through CMD analysis of optical (*Hubble space Telescope*) photometry obtained in a few small regions in the centres and outskirts of the Magellanic Clouds. They argued that the relative enhancement in the SFH of the SMC is a consequence of the interaction with the LMC, with a stronger impact on the global star formation of the SMC due to its much smaller mass compared to the LMC. The smaller size of the SMC may also have resulted in the slower assembly at early times, similar to what was found in M33 (Javadi et al. 2011). This would be easier to understand if the SMC and LMC did not form as a pair, but at least the SMC was formed in isolation.

A secondary peak of the SFH for the central part of the LMC has been reported in other studies, e.g. Smecker-Hane et al. (2002) who found a dominant star formation activity within the bar of the LMC at intermediate ages. Having isolated the SFH of the bar of the LMC from that of the disc, it has become clear that the bar formed a few Gyr ago and has maintained its star formation until very recently
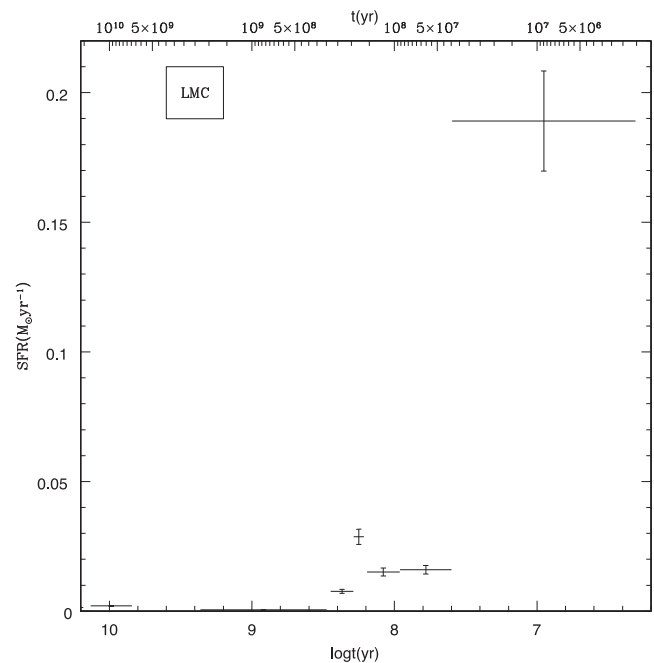

Figure 9. Recent star formation of the LMC using Ulaczyk et al. (2013) catalogue of more massive (brighter) stars.

(∼200 Myr). However, the secondary peak in SFR in the SMC is much sharper (in duration) and occurred ∼700 Myr ago. There is indeed a similar peak noticeable in the SFH of the LMC, and this is thus distinct from the star formation activity related to the bar itself. The co-eval 700-Myr bursts in the SMC and LMC are arguably due to the tidal interaction between the Magellanic Clouds and possibly their approach of the Milky Way (cf. Bekki & Chiba 2005; Indu & Subramaniam 2011).

The LMC catalogues we have worked with are limited to $t \sim 100$ Myr due to the lack of more massive stars (brighter stars) because of saturation of the detectors used in the surveys. However, Ulaczyk et al. (2013) presented a catalogue of brighter stars that had been saturated in the main OGLE catalogue. On the basis of this bright sample, we derive the recent SFH in the LMC using the methods described above (Fig. 9). We find an SFR of ≈0.19 $M_\odot$ yr^{-1} at $t \sim 5$ Myr, i.e. similar to that over the past few Gyr or so (compare, for instance, with Fig. 4).

After applying a correction to the pulsation duration of LPVs as predicted by the stellar evolutionary models (see Javadi et al. 2013), the resulting SFRs are now in very good agreement with those obtained in other studies (e.g. Harris & Zaritsky 2004, 2009; Cignoni et al. 2012). However, a recent investigation by the Padova group of their own models revealed a severe overestimation of the lifetimes of thermal-pulsing AGB stars (Girardi et al. 2013) which could also have implications for the duration of the radial pulsation phase. Indeed, the techniques we have pioneered in M33 (Javadi et al. 2011, 2013), and now applied in the Magellanic Clouds, offer a promising avenue towards exposing the assembly and development of galaxies as well as improving models for the late stages of stellar evolution and mass-loss.

REFERENCES

Bekki K., Chiba M., 2005, MNRAS, 356, 680

Bertelli G., Mateo M., Chiosi C., Bressan A., 1992, ApJ, 388, 400

Cignoni M., Cole A. A., Tosi M., Gallagher J. S., Sabbi E., Anderson J., Grebel E. K., Nota A., 2012, ApJ, 754, 130

Cignoni M., Cole A. A., Tosi M., Gallagher J. S., Sabbi E., Anderson J., Grebel E. K., Nota A., 2013, ApJ, 775, 83

Cioni M.-R. L. et al., 2014, A&A, 562, A32

Freedman W. L., Kennicutt R. C., Mould J. R., 2010, Highlights of Astronomy, 15, 1

Gieren W., Storm J., Barnes T. G., III, Fouqué P., Pietrzyński G., Kienzle F., 2005, ApJ, 627, 224

Girardi L., Marigo P., Bressan A., Rosenfield P., 2013, ApJ, 777, 142

Harris J., Zaritsky D., 2004, AJ, 127, 1531

Harris J., Zaritsky D., 2009, AJ, 138, 1243

Haschke R., Grebel E. K., Duffau S., 2011, AJ, 141, 1865

Hilditch R. W., Howarth I. D., Harries T., 2005, MNRAS, 357, 304

Hodge P. W., 1960, ApJ, 132, 341

Indu G., Subramaniam A., 2011, A&A, 535, A115

Ita Y. et al., 2004a, MNRAS, 347, 720

Ita Y. et al., 2004b, MNRAS, 353, 705

Javadi A., van Loon J. Th., Mirtorabi M. T., 2011, MNRAS, 414, 3394

Javadi A., van Loon J. Th., Khosroshahi H., Mirtorabi M., 2013, MNRAS, 432, 2824

Kroupa P, 2001, N, 322, 231

Luri X., Gomez A. E., Torra J., Figueras F., Mennessier M. O., 1998, A&A, 335, 81

Macri L. M., Stanek K. Z., Bersier D., Greenhill L. J., Reid M. J., 2006, ApJ, 652, 1133

Marigo P., Girardi L., Bressan A., Groenewegen M. A. T., Silva L., Granato G. L., 2008, A&A, 482, 883

Meschin I., Gallart C., Aparicio A., Hidalgo S. L., Monelli M., Stetson P. B., Carrera R., 2014, MNRAS, 438, 1067

Monelli M. et al., 2011, EAS Publ. Ser., 48, 43

Ripepi V. et al., 2014, MNRAS, 442, 1897

Sagar R., Pandey A. K., 1989, A&AS, 79, 407

Smecker-Hane T. A., Cole A., Gallagher J. S., Stetson P., 2002, ApJ, 566, 239

Soszyński I. et al., 2011, Acta Astron., 61, 217

Spano M., Mowlavi N., Eyer L., Burki G., Marquette J.-B., Lecoeur-Tabi I., Tisserand P., 2011, A&A, 536, A60

Subramanian S., Subramaniam A., 2011, in Khare P., Ishwara-Chandra C. H., eds, Proc. 29th ASI Conf. Ser. Vol. 3, The 3D Structure of the Small Magellanic Cloud. Astron. Soc. India, Pune, p. 144

Ulaczyk K. et al., 2013, Acta Astron., 63, 159

van Loon J. Th., Zijlstra A. A., Whitelock P. A., Waters L. B. F. M., Loup C., Trams N. R., 1997, A&A, 325, 585

van Loon J. Th., Cohen M., Oliveira J. M., Matsuura M., McDonald I., Sloan G. C., Wood P. R., Zijlstra A. A., 2008, A&A, 487, 1055

Weisz D. R. et al., 2013, MNRAS, 431, 364

Whitelock P. A., Feast M. W., van Loon J. Th., Zijlstra A. A., 2003, MNRAS, 342, 86

Wood P. R., Whiteoak J. B., Hughes S. M. G., Bessell M. S., Gardner F. F., Hyland A. R., 1992, ApJ, 397, 552

This paper has been typeset from a TeX/LaTeX file prepared by the author.